

Search and study of young infrared stellar clusters

Naira Azatyan^{1*}

^{1*}Byurakan Astrophysical Observatory, 0213 Aragatsotn Prov., Armenia.

Corresponding author(s). E-mail(s): nayazatyan@bao.sci.am;

Abstract

The main aim of this paper is to study both the Interstellar Medium (ISM) and the young stellar population in the three star-forming regions, namely IRAS 05137+3919, 05168+3634, and 19110+1045. The study of the ISM includes determination of the hydrogen column density ($N(\text{H}_2)$) and dust temperature (T_d) in the regions using Modified blackbody fitting. The main parameters of identified and classified young stellar objects (YSOs) belonging to the regions were determined comparing with the radiation transfer models. We also constructed a colour-magnitude diagram to compare the parameters of the YSOs with the results of the radiative transfer models. The three stellar populations appear to have formed under different scenarios. In the cases of IRAS 05137+3919 and IRAS 05168+3634, the age spread is considerably wider, suggesting that the stellar population likely emerged from independent condensations. In contrast, the third region comprises a pair of ultra-compact HII regions (UCHIIs), G45.12+0.13 and G45.07+0.13, with a notably smaller age spread. This hints at the possibility that these clusters originated from a single triggering event.

Keywords: stars: pre-main sequence – infrared: stars – radiative transfer - Interstellar medium (ISM)

1 Introduction

The process of star formation remains ongoing throughout various stages of evolution of our galaxy and other galaxies, even in the present era [Ambartsumian \(1947\)](#). It stands as one of the most pivotal processes that yield observable outcomes within galaxies. Giant molecular clouds are birthplaces of stellar population ([Soderblom, 2010](#)). Stellar clusters that remain embedded within their original molecular clouds hold a special significance. They provide insights into distinguishing the characteristics

of stellar clusters related to their birth conditions from those derived from subsequent evolution (Lada and Lada, 2003). Therefore, there exists a genetic connection between young stellar objects (YSOs) and surrounding Interstellar Medium (ISM). It necessitates an integrated approach to study star-forming regions which implies determination of the main properties of already formed young stellar clusters and the surrounding environment. Moreover, the integrated approach to study of embedded stellar clusters can provide information about the initial star formation scenarios. When star formation within clusters is triggered, one would expect a limited age spread among the stars within the cluster. Conversely, in protocluster condensations that initiate star formation independently, individual clumps are likely to exhibit a broader age distribution (e.g. Preibisch, 2012).

This paper presents findings of detailed investigation of young stellar clusters in the three star-forming regions: IRAS 05137+3919, 05168+3634, and 19110+1045 with a substantial size and multi-component structures. All three regions are active knots for star formation. Figure 1 shows colour-composite images of the three star-forming regions with combinations of different wavelength range images. For each of these regions, an exhaustive analysis was undertaken, covering the following topics: 1) determining ISM parameters, specifically the distribution of hydrogen column density ($N(H_2)$) and dust temperature (T_d); 2) the search for young stellar clusters; 3) identifying cluster members by examining their infrared characteristics; and 4) determining the age and age spread among the members within these clusters. This paper is essentially a generalization of the results presented in a series of works devoted to the above-mentioned topics (Nikoghosyan and Azatyan, 2014; Azatyan et al, 2016; Azatyan and Nikoghosyan, 2018; Azatyan, 2019; Nikoghosyan et al, 2020; Azatyan et al, 2020; Nikoghosyan et al, 2021; Azatyan et al, 2022) which were the basis for my PhD thesis.

We have organised the paper as follows. Section 2 describes the used data and methods; in Section 3, we analyse the stellar population and ISM properties in the regions. Finally, the study results are summarised in Section 4.

2 Used data and methods

The study encompasses two primary scientific focuses: the examination of the ISM and the analysis of YSOs. For this purpose, we used data covering a wide range of near- to far-infrared (NIR, FIR) wavelengths.

For the determination of $N(H_2)$ and T_d in the three star-forming regions, we used *Herschel* FIR images, covering the optically thin spectral range of 160–500 μm obtained on the Photodetector Array Camera and Spectrometer (PACS, Poglitsch et al, 2010) and the Spectral and Photometric Imaging Receiver (SPIRE, Griffin et al, 2010). These spectral ranges are most productive for determining the parameters of the cold ISM in molecular clouds. Dust emission in the FIR can be modelled as a modified blackbody $I_\nu = k_\nu \mu_{H_2} m_H N(H_2) B_\nu(T_d)$, where k_ν is the dust opacity, $\mu_{H_2} = 2.8$ representing the mean weight per hydrogen molecule (Kauffmann et al, 2008), m_H is the mass of hydrogen, $N(H_2)$ is the hydrogen column density, and $B_\nu(T_d)$ is the Planck function at the dust temperature T_d . The dust opacity in the FIR is usually

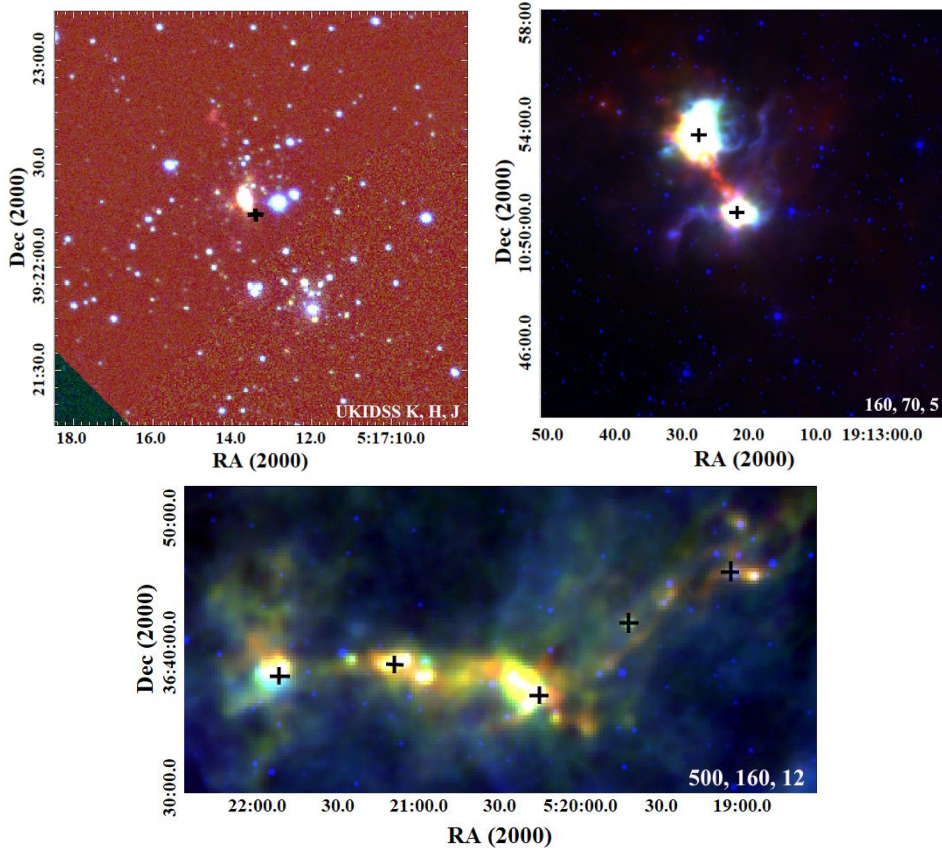


Fig. 1 (*Left*) A colour-composite image of the IRAS 05137+3919 star-forming region, combining data of UKIDSS J (in blue), H (in green), and K (in red). The position of the IRAS source is marked by a black cross. (*Right*) A colour-composite image of the G45.12+0.13 and G45.07+0.13 UCHII regions, combining data of Spitzer 5.0 μm (in blue), Herschel 70 μm (in green), and Herschel 160 μm (in red). The positions of the IRAS sources are marked by black crosses and they are in the following order from up to down: IRAS 19111+1048 and 19110+1045. (*Bottom*) A colour-composite image of the IRAS 05168+3634 star-forming region, combining data of WISE 12 μm (in blue), Herschel 160 μm (in green), and Herschel 500 μm (in red). The positions of the IRAS sources are marked by black crosses and they are in the following order from the left to the right: IRAS 05184+3635, 05177+3636, 05168+3634, 05162+3639, and 05156+3643.

parametrized as a power law normalised to the value k_0 at a reference frequency ν_0 , so $k_\nu = k_0(\nu/\nu_0)^\beta \text{cm}^{-2}\text{g}^{-1}$. Following Hildebrand (1983), Könyves et al (2015), we adopted $k_0 = 0.1 \text{cm}^{-2}\text{g}^{-1}$ at 300 μm (gas-to-dust ratio of 100) and $\beta = 2$. Roy et al (2014) showed that this assumption is good within better than 50% in the bulk of molecular clouds. Based on the discussion in previous studies (e.g. Battersby et al, 2011), we excluded the 70 μm data as the optically thin assumption may not hold. In addition, the emission here would have a significant contribution from a warm dust component, thus, modelling with a single-temperature blackbody would over-estimate the derived temperature. The three shortward intensity maps were degraded to the

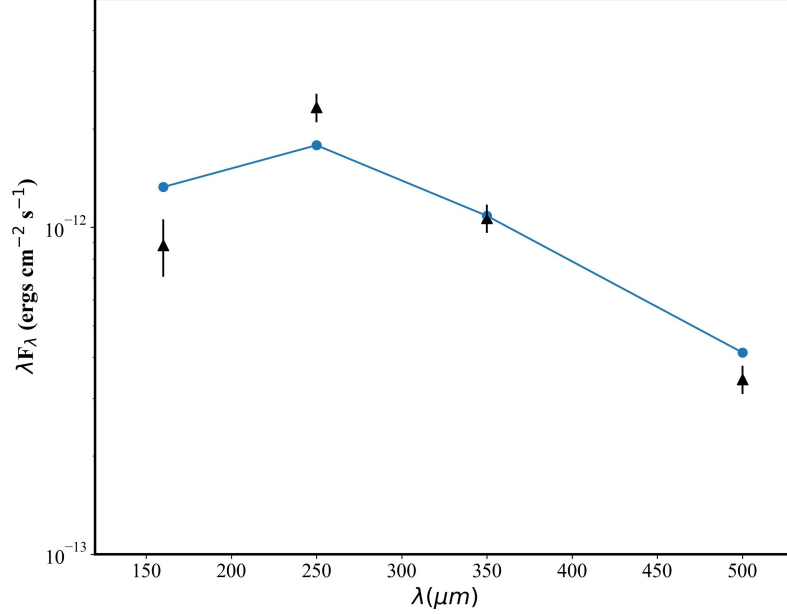


Fig. 2 A blackbody fitting of a low dust temperature (11 K) in IRAS 05137+3919 star-forming region. The filled triangles represent the observed fluxes in *Herschel* four bands with their error bars, while filled circles represent the fluxes predicted by the model in the same bands. The blue line shows the fit of the predicted fluxes. The uncertainties between two samples is 0.024.

spatial resolution of the 500 μm band; the four maps were then translated to a common coordinate system using 14" pixels at all wavelengths. The SED fitting procedure for the cold ISM was executed pixel by pixel. Following to Pezzuto et al (2021), we created a grid of models by varying only the temperature, in the range $5 \leq T_d(K) \leq 50$, in step of 0.01 K and for each temperature T_j , the code computes the intensity at FIR wavelengths for all bands. Since the intensity I_ν is linear with $N(H_2)$, we can compute the column density at each pixel using a straightforward application of the least-squares technique. The uncertainty of I_ν for SPIRE is 10% and for PACS is 20% (Könyves et al, 2015). Figure 2 shows an example of blackbody fitting for low dust temperature (11 K) in IRAS 05137+3919 star-forming region. The uncertainties between the observed and predicted fluxes is 0.024 for this particular pixel.

For the second task that is the analysis of YSOs, we used data spanning the NIR, mid-infrared (MIR), and FIR wavelengths. For this task, it was used the data of Galactic Plane Survey DR6 (UKIDSS GPS, Lucas et al, 2008), Two Micron Sky Survey (2MASS, Cutri et al, 2003), Galactic Legacy Infrared Midplane Survey Extraordinaire (GLIMPSE) and GLIMPSE 360 (Churchwell et al, 2009), Multiband Infrared Photometer for *Spitzer* (MIPSGAL, Carey et al, 2009), Wide-field Infrared Survey Explorer (WISE, Wright et al, 2010), Midcourse Space Experiment (MSX, Price et al, 2001), *Herschel* PACS, SPIRE, *Herschel* Infrared Galactic Plane Survey (Hi-GAL, Molinari et al, 2016), and the Infrared Astronomical Satellite (IRAS, Neugebauer et al, 1984) Point Source Catalog v2.1 (PSC) catalogs. UKIDSS-DR6 catalog was selected

as a primary. Then, this catalog was cross-matched with other MIR and FIR catalogs, using a matching radius of 3σ , accounting for the combined error. Since, the presence of circumstellar discs and envelopes cause an infrared (IR) excess of a YSO, therefore YSO candidates were identified based on their position in colour–colour (c-c) IR diagrams. The choice of colours relied on the availability of data. We employed two c-c diagrams, specifically (J-H) versus (H-K) and (J-K) versus [3.6]-[4.5], to identify YSOs within the IRAS 05137+3919 star-forming region. Then, the selection of YSOs in the IRAS 05168+3634 star-forming region was guided by the analysis of four c-c diagrams, specifically (J-H) versus (H-K), K-[3.6] versus [3.6]-[4.5], [3.4]-[4.6] versus [4.6]-[12], and [3.4]-[4.6] versus [4.6]-[22]. Finally, the selection of YSOs in the IRAS 19110+1045 star-forming region involved the utilization of six c-c diagrams, specifically (J-H) versus (H-K), K-[3.6] versus [3.6]-[4.5], [3.6]-[4.5] versus [5.8]-[8.0], [3.6]-[5.8] versus [8.0]-[24], [3.4]-[4.6] versus [4.6]-[12], and [3.4]-[4.6] versus [4.6]-[22]. To validate the selected YSOs and extract their essential characteristics, we constructed their spectral energy distributions (SEDs) and compared them with radiative transfer models developed by [Robitaille \(2017\)](#). Fig. 7 in [Azatyan \(2019\)](#) shows examples of such a comparison for the YSOs associated with IRAS sources in the IRAS 05168+3634 region.

Table 1 The parameters of ISM and stellar population in the star-forming regions

IRAS	α (2000) (hh mm ss)	δ (2000) (dd mm ss)	$N(\text{H}_2)$ ($\times 10^{23} \text{ cm}^{-2}$)	T_d (K)	YSOs	Radius (pc)	D (kpc)	A_v (mag)
(1)	(2)	(3)	(4)	(5)	(6)	(7)	(8)	(9)
05137+3919	05 17 13.3	+39 22 14.0	0.25 – 1.0	11 – 22	33	1.9/4.8	4.4/11	1.8
05184+3635	05 21 53.2	+36 38 20.4	1.1 – 1.5	12 – 15	52	1.4	1.9	1.4
05177+3636	05 21 09.4	+36 39 37.1	1.1 – 2.3	12 – 13	79	1.9	1.9	1.3
05168+3634	05 20 16.4	+36 37 18.7	1.1 – 3.8	11 – 24	57	1.7	1.9	4.5
05162+3639	05 19 38.4	+36 42 25.0	0.9 – 1.0	11 – 12	5	0.14	1.9	1.2
05156+3643	05 19 03.6	+36 46 15.7	1.1 – 1.6	11 – 12	47	1.5	1.9	1.0
19110+1045	19 13 22.0	+10 50 54.0	3.0 – 5.0	18 – 42	37	1.8	7.8	13
19111+1048	19 13 27.8	+10 53 36.7	3.0 – 5.5	18 – 35	87	2.7	7.8	13

Note: (1)-names of (sub-)regions, (2),(3)- coordinates of the IRAS sources, (4)- ranges of hydrogen column density, (5)- ranges of dust temperature, (6)- numbers of YSOs within the selected radii, (7)-the radii of (sub-)regions, (8)- adopted distances of the regions, (9)- the median interstellar extinctions estimated with SED fitting tool for IRAS 05137+3919 and 19110+1045&19111+1048 star-forming regions, and according to the COBE/DIRBE and IRAS/ISSA maps ([Schlegel et al, 1998](#)) for IRAS 05168+3634 star-forming region.

3 Results and Discussion

The selected regions (IRAS 05137+3919, 05168+3634, and 19110+1045), among other things, hold particular interest due to their considerable distances, providing an opportunity to evaluate the capabilities of the databases we have access to. For the IRAS 05137+3919, the distance estimates based on radio observations have a large variation: from ~ 4.4 kpc ([Casoli et al, 1986](#); [Wouterloot and Brand, 1989](#)) to 10.8 kpc ([Molinari et al, 1996](#)). The distance estimations of IRAS 05168+3634 star-forming region are also different: 6.08 kpc ([Molinari et al, 1996](#)) and $1.88^{+0.21}_{-0.17}$ kpc ([Sakai et al, 2012](#)). Given the significant discrepancy in the distance estimates for the IRAS 05168+3634 star-forming region, we attempted to identify YSOs within the

Gaia EDR3 database. The results obtained from the *Gaia* EDR3 data provide additional support to that this star-forming region is situated at a distance of ~ 1.9 kpc (Nikoghosyan et al, 2021). And finally, the distance estimate for the IRAS 19110+1045 star-forming region is 7.75 ± 0.45 kpc (Wu et al, 2019). Table 1 contains the parameters of ISM and stellar population in the star-forming regions and below are the results of their study.

In the vicinity of **IRAS 05137+3919**, we observed a young stellar cluster closely associated with the CPM15 YSO (Campbell et al, 1989) (Figure 1 top left). This region exhibits various signs of active star formation, including maser emissions, as well as the presence of CO and H₂ outflows (Zhang et al, 2005; Varricatt et al, 2010). The results of modified single-temperature blackbody fitting are presented in (4) and (5) Columns of Table 1. The maxima for both N(H₂) and T_d coincide with the position of the IRAS source. Within determined 1.5' radius, we identify 33 YSOs using two c-c diagrams. We were able to derive the parameters of these YSOs using the SED fitting tool. These selected YSOs exhibit a non-uniform distribution within the star-forming region, forming two distinct subgroups. One of these subgroups is situated around CPM 15, while the second group encompasses a notable number of middle-mass objects, surrounded by gas-dust nebulae (Nikoghosyan and Azatyan, 2014).

The next young stellar cluster is concentrated around the **IRAS 05168+3634** source. The presence of diverse maser emissions and the existence of ¹³CO cores provide compelling evidence of its ongoing star-forming activity (Zhang et al, 2005; Fontani et al, 2010; Guan et al, 2008). Notably, in the FIR wavelengths, the region exhibits a more intricate and complex structure compared to its appearance in the NIR, as illustrated in bottom panel of Figure 1. Our investigation of the whole star-forming region within the molecular cloud unveiled the presence of four additional IRAS sources at the same distance, namely IRAS 05184+3635, 05177+3636, 05162+3639, and 05156+3643, which are embedded into a ~ 26 pc long cloud complex (Azatyan, 2019). The results of modified single-temperature blackbody fitting are presented in Table 1 for each IRAS sub-region. Notably, the relatively warmer gas-dusty material leads to dense condensations around the IRAS objects (Nikoghosyan et al, 2021). An exception is IRAS 05162+3639 sub-region where the N(H₂) map reveals a distinct absence of regions with relatively higher density. Additionally, no cluster of YSOs has been identified around this source; instead, only five stars are present. Within determined radii, we identify YSOs using four c-c diagrams and the results are presented in (6) Column of Table 1 for each IRAS sub-region. Comprehensive tables containing information on the selected YSOs, including their NIR, MIR, and FIR photometry, as well as parameters obtained through the SED fitting tool, can be accessed via the VizieR On-line Data Catalog¹ (Azatyan, 2019).

The final star-forming region is associated with the **IRAS 19110+1045** and **19111+1048** sources, which are commonly referred to as the **G45.07+0.13** and **G45.12+0.13** UCHII regions, respectively. This system serves as an ideal laboratory

¹The full tables are available in the VizieR On-line Data Catalog: J/A+A/622/A38

for the exploration of the initial phases of massive star formation and their impact on their surrounding environments. Figure 1 top right panel shows colour-composite image of the region and it also indicates that these UCHII regions are interconnected by a relatively cooler bridge, strongly suggesting that they form a physically linked system. The results of modified single-temperature blackbody fitting are presented in Table 1 for each IRAS sub-region. In the G45.07+0.13 region, the IRAS source is slightly offset from the density peak, while in the G45.12+0.13 region, the position of IRAS 19111+1048 coincides with the maxima of both T_d and $N(\text{H}_2)$. Let us note that in this star-forming region both T_d and $N(\text{H}_2)$ are the highest. Within determined radii, we identify YSOs using six c-c diagrams and the results are presented in (6) Column of Table 1 for each IRAS sub-region. As in the previous cases, we included objects classified as YSOs in at least two c-c diagrams into our list. However, due to the presence of two saturated areas in the MIR band surrounding the IRAS sources (IRAS 19110+1045 with a 25'' radius and IRAS 19111+1048 with a 50'' radius), objects within those regions were classified as YSO candidates based solely on the NIR c-c diagram and we conducted a visual inspection of the YSO candidates (95 YSOs) in the two MIR-saturated regions, as these objects are of particular interest due to their proximity to the UCHIIs. The comprehensive tables containing information on the selected YSOs, including their NIR, MIR, and FIR photometry, as well as parameters derived from SED fitting tool, can be accessed in the VizieR On-line Data Catalog². Among considered three star-forming regions, massive stars were only detected in this one. In the G45.07+0.13 region, we identified two massive stars, while in the G45.12+0.13 region - four, and one of them with a mass of $9.4 \pm 4.3 M_\odot$, a temperature of $23\,000 \pm 11\,000$ K, and an evolutionary age of $(2.5 \pm 1.2) \times 10^6$ years was successfully identified as the NIR counterpart of the IRAS 19111+1048 source (Azatyan et al, 2022).

Figure 3 bottom panel shows the distribution of the identified YSOs in the colour-magnitude diagram (CMD). The correction of J and K magnitudes of the YSOs for each region was done with the median interstellar extinctions and the adopted distances taken from Table 1. For IRAS 05137+3919, we used only 4.4 kpc distance. The members of each star-forming regions are indicated with different colours and symbols. As we can see, the members of each star-forming regions display different dispersion concerning the isochrones (solid thin and thick lines). The members in IRAS 05137+3919 and 05168+3634 star-forming regions show large dispersion concerning the isochrones, while the members in IRAS 19110+1045 and 19111+1048 star-forming regions display relatively low dispersion concerning the isochrones and they are more evolved. To enhance clarity, the histograms for $(J - K)_{abs}$ are presented in the top panel with the same colours as in bottom panel. In general, the stellar objects in IRAS 05137+3919 and 05168+3634 star-forming regions, display large spreads in $(J - K)_{abs}$, while the members in IRAS 19110+1045 and 19111+1048 star-forming regions are mostly concentrated. For the comparison, we also constructed the histograms of the evolutionary ages for the members of the star-forming regions based

²The complete dataset is accessible in the VizieR On-line Data Catalog: [J/other/PASA/39.24](https://vizier.cesr.fr/vizieR/)

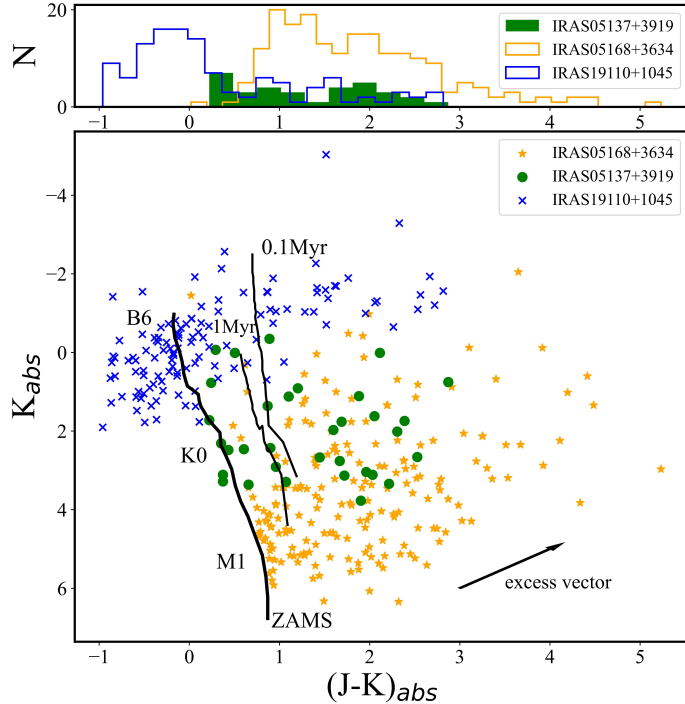


Fig. 3 (*Bottom*) K versus (J-K) CMDs for the identified YSOs in the three star-forming regions. In these diagram, blue crosses represent stellar objects in the IRAS 19110+1045 and 19111+1048 star-forming regions labelled as IRAS 19110+1045, green circles represent objects located in the IRAS 05137+3919 star-forming region, and finally yellow stars represent stellar objects in IRAS 05168+3634 star-forming region. The pre-main sequence isochrones for the 0.1 and 1 Myr (Siess et al, 2000) and ZAMS are drawn as solid thin and thick lines, respectively. The positions of a few spectral types are labelled. The J and K magnitudes of the YSOs are corrected for the median interstellar extinctions and distances separately. The solid arrow indicates the average slope of NIR excesses caused by circumstellar discs (López-Chico and Salas, 2007). (*Top*) Histograms of $(J - K)_{abs}$ values of the three star-forming regions with the same colours.

on the results of the SED fitting tool. Figure 4 presents histograms of the evolutionary ages with the same colours as in Figure 3. The histograms revealed a notably wide spread for all regions. It should be noted, the evolutionary age distribution for the objects in IRAS 19110+1045 and 19111+1048 star-forming regions (blue bars) is derived from parameters obtained for only 29 YSOs subjected to the SED fitting tool. Most of the remaining 95 YSOs within the MIR-saturated regions are concentrated around the zero-age main sequence (ZAMS) and situated to the left of the 1 Myr isochrone. Consequently, it is posited that these objects significantly contribute to the first peak in the evolutionary age distribution, rendering it a single, well-defined peak similar to the $(J - K)_{abs}$ histogram. Consequently, the large age spread observed in the IRAS 05137+3919 and 05168+3634 star-forming regions provides strong evidence to support the conclusion that the stellar populations within them are the outcome of independent condensations within the parent molecular cloud. In contrary, the small spread of evolutionary ages in IRAS 19110+1045 and 19111+1048 star-forming regions

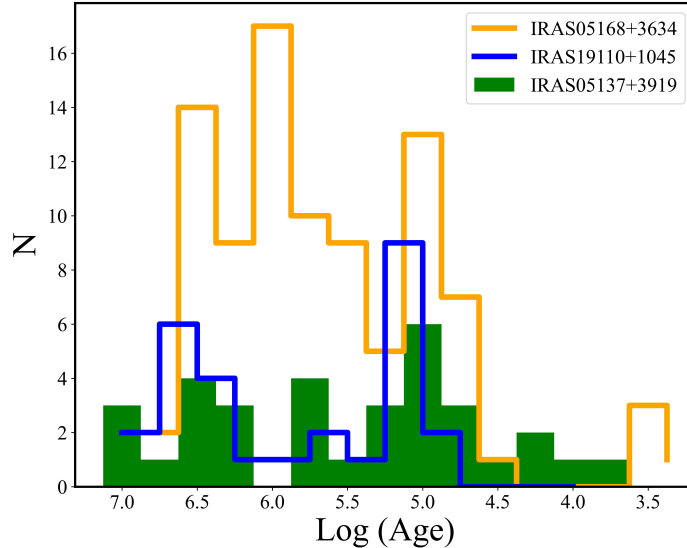


Fig. 4 Histograms of the evolutionary ages for members of the three star-forming regions. The colours are the same as in Figure 3. The bin size corresponds to $\text{Log}(\text{Age}) = 0.25$.

suggests that formation of the stellar population may be attributed to a triggering shock. We assume that Granat 1915+105 High Mass X-ray Binary which is located at the same distance as IRAS 19110+1045 and 19111+1048 star-forming regions and belongs to the same molecular cloud could be the possible trigger of the star formation in these regions. We plan to check the reliability of this assumption in our future work.

4 Conclusion

Here are the main findings from the detailed study of the IRAS 05137+3919, 05168+3634, 19110+1045&19111+1048 star-forming regions:

- A total of 33 YSOs were identified in the IRAS 05137+3919 region, 240 YSOs in the IRAS 05168+3634 region, and totally, 124 YSOs in the IRAS 19110+1045 and 19111+1048 regions.
- In the IRAS 05137+3919 star-forming region, the selected YSOs are not uniformly distributed and form two distinct subgroups.
- In the IRAS 05168+3634 field, five dense subgroups were detected around IRAS sources, indicating that IRAS 05168+3634 and four other sub-regions are embedded into a ~ 26 pc long cloud complex, located at ~ 1.9 kpc distance based on *Gaia* EDR3 parallax measurements.
- Both IRAS 05137+3919 and IRAS 05168+3634 star-forming regions exhibit a wide age spread, suggesting that the stellar populations within these regions formed independently within the parent molecular clouds.
- The members of the IRAS clusters in the G45.12+0.13 and G45.07+0.13 UC HII regions show low scatter relative to the isochrones, and their age distribution indicates a small spread, possibly related to an external triggering shock.

- Among the considered star-forming regions, massive stars were only detected in the region where star formation may have been triggered and the temperature and hydrogen column density of the ISM are the highest, specifically IRAS 19110+1045 and 19111+1048.

These findings provide valuable insights into the structure, formation, and age distribution of stars within these star-forming regions.

Acknowledgments. I thank the anonymous reviewer for constructive comments and suggestions. I would like to thank my supervisor – Dr. Elena Nikoghosyan for her invaluable supervision and support during the course of my PhD degree. This work partially was made possible by a research grant number № 21AG-1C044 from Science Committee of Ministry of Education, Science, Culture and Sports RA.

References

- Ambartsumian VA (1947) The evolution of stars and astrophysics
- Azatyany N, Nikoghosyan E, Harutyunian H, et al (2020) Stellar population in two star-forming regions. *Communications of the Byurakan Astrophysical Observatory* 67:211–218. <https://doi.org/10.52526/25792776-2020.67.2-211>
- Azatyany N, Nikoghosyan E, Harutyunian H, et al (2022) Infrared study of the star-forming region associated with the UC HII regions G45.07+0.13 and G45.12+0.13. *Publ Astron Soc Aust* 39:e024. <https://doi.org/10.1017/pasa.2022.20>, [arXiv:2204.06338](https://arxiv.org/abs/2204.06338) [astro-ph.SR]
- Azatyany NM (2019) Investigation of the stellar content in the IRAS 05168+3634 star-forming region. *Astronomy & Astrophysics* 622:A38. <https://doi.org/10.1051/0004-6361/201731904>, [arXiv:1812.06808](https://arxiv.org/abs/1812.06808) [astro-ph.SR]
- Azatyany NM, Nikoghosyan EH (2018) Investigation of the stellar content in the IRAS 05168+3634 star-forming region. *Communications of the Byurakan Astrophysical Observatory* 65(2):228–239. <https://doi.org/10.52526/25792776-2018.2.2-228>
- Azatyany NM, Nikoghosyan EH, Khachatryan KG (2016) Search for Compact Stellar Groups in the Vicinity of Iras Sources. *Astrophysics* 59:339–353. <https://doi.org/10.1007/s10511-016-9439-4>, [arXiv:1608.02225](https://arxiv.org/abs/1608.02225) [astro-ph.SR]
- Battersby C, Bally J, Ginsburg A, et al (2011) Characterizing precursors to stellar clusters with Herschel. *Astronomy & Astrophysics* 535:A128. <https://doi.org/10.1051/0004-6361/201116559>, [arXiv:1101.4654](https://arxiv.org/abs/1101.4654) [astro-ph.GA]
- Campbell B, Persson SE, Matthews K (1989) Identifications of New Young Stellar Objects Associated with IRAS Point Sources. III. The Northern Galactic Plane. *Astronomical Journal* 98:643. <https://doi.org/10.1086/115164>
- Carey SJ, Noriega-Crespo A, Mizuno DR, et al (2009) MIPS GAL: A Survey of the Inner Galactic Plane at 24 and 70 μm . *Publ Astron Soc Pac* 121(875):76. <https://doi.org/10.1086/589888>

[//doi.org/10.1086/596581](https://doi.org/10.1086/596581)

- Casoli F, Dupraz C, Gerin M, et al (1986) 13CO and 12CO observations of cold IRAS unidentified point sources in the galaxy. *Astronomy & Astrophysics* 169:281–297
- Churchwell E, Babler BL, Meade MR, et al (2009) The Spitzer/GLIMPSE Surveys: A New View of the Milky Way. *Publ Astron Soc Pac* 121:213–230. <https://doi.org/10.1086/597811>
- Cutri RM, Skrutskie MF, van Dyk S, et al (2003) VizieR Online Data Catalog: 2MASS All-Sky Catalog of Point Sources (Cutri+ 2003). *VizieR Online Data Catalog* II/246
- Fontani F, Cesaroni R, Furuya RS (2010) Class I and Class II methanol masers in high-mass star-forming regions. *Astronomy & Astrophysics* 517:A56. <https://doi.org/10.1051/0004-6361/200913679>, [arXiv:1004.3689](https://arxiv.org/abs/1004.3689) [astro-ph.GA]
- Griffin MJ, Abergel A, Abreu A, et al (2010) The Herschel-SPIRE instrument and its in-flight performance. *Astronomy & Astrophysics* 518:L3. <https://doi.org/10.1051/0004-6361/201014519>, [arXiv:1005.5123](https://arxiv.org/abs/1005.5123) [astro-ph.IM]
- Guan X, Wu Y, Ju B (2008) A mapping survey of massive CO cores. *Mon Not R Astron Soc* 391(2):869–880. <https://doi.org/10.1111/j.1365-2966.2008.13937.x>
- Hildebrand RH (1983) The determination of cloud masses and dust characteristics from submillimetre thermal emission. *QJRAS* 24:267–282
- Kauffmann J, Bertoldi F, Bourke TL, et al (2008) MAMBO mapping of Spitzer c2d small clouds and cores. *Astronomy & Astrophysics* 487(3):993–1017. <https://doi.org/10.1051/0004-6361:200809481>, [arXiv:0805.4205](https://arxiv.org/abs/0805.4205) [astro-ph]
- Könyves V, André P, Men'shchikov A, et al (2015) A census of dense cores in the Aquila cloud complex: SPIRE/PACS observations from the Herschel Gould Belt survey. *Astronomy & Astrophysics* 584:A91. <https://doi.org/10.1051/0004-6361/201525861>, [arXiv:1507.05926](https://arxiv.org/abs/1507.05926) [astro-ph.GA]
- Lada CJ, Lada EA (2003) Embedded Clusters in Molecular Clouds. *Ann Rev Astron Astrophys* 41:57–115. <https://doi.org/10.1146/annurev.astro.41.011802.094844>, [astro-ph/0301540](https://arxiv.org/abs/astro-ph/0301540)
- López-Chico T, Salas L (2007) Mass determination for T Tauri stars from JHK Photometry. *Rev Mex Astron Astrofis* 43:155–171. [astro-ph/0611721](https://arxiv.org/abs/astro-ph/0611721)
- Lucas PW, Hoare MG, Longmore A, et al (2008) The UKIDSS Galactic Plane Survey. *Mon Not R Astron Soc* 391:136–163. <https://doi.org/10.1111/j.1365-2966.2008.13924.x>, [arXiv:0712.0100](https://arxiv.org/abs/0712.0100)
- Molinari S, Brand J, Cesaroni R, et al (1996) A search for precursors of ultracompact HII regions in a sample of luminous IRAS sources. I. Association with ammonia

cores. *Astronomy & Astrophysics* 308:573–587

- Molinari S, Schisano E, Elia D, et al (2016) Hi-GAL, the Herschel infrared Galactic Plane Survey: photometric maps and compact source catalogues. First data release for the inner Milky Way: $+68^\circ \geq l \geq -70^\circ$. *Astronomy & Astrophysics* 591:A149. <https://doi.org/10.1051/0004-6361/201526380>, [arXiv:1604.05911](https://arxiv.org/abs/1604.05911) [astro-ph.GA]
- Neugebauer G, Habing HJ, van Duinen R, et al (1984) The Infrared Astronomical Satellite (IRAS) mission. *Astrophysical Journal* 278:L1–L6. <https://doi.org/10.1086/184209>
- Nikoghosyan E, Azatyan N, Harutyunian H, et al (2020) Properties of ISM in two star-forming regions. *Communications of the Byurakan Astrophysical Observatory* 67:187–192. <https://doi.org/10.52526/25792776-2020.67.2-187>
- Nikoghosyan EH, Azatyan N (2014) Young Stellar Cluster in the Vicinity of the IRAS 05137+3919 Source. *Astrophysics* 57(3):330–343. <https://doi.org/10.1007/s10511-014-9338-5>
- Nikoghosyan EH, Azatyan NM, Andreasyan DH, et al (2021) The structure of the IRAS05168+3634 star-forming region. *Astrophys Space Sci* 366(11):114. <https://doi.org/10.1007/s10509-021-04023-4>, [arXiv:2111.02906](https://arxiv.org/abs/2111.02906) [astro-ph.GA]
- Pezzuto S, Benedettini M, Di Francesco J, et al (2021) Physical properties of the ambient medium and of dense cores in the Perseus star-forming region derived from Herschel Gould Belt Survey observations. *Astronomy & Astrophysics* 645:A55. <https://doi.org/10.1051/0004-6361/201936534>, [arXiv:2010.00006](https://arxiv.org/abs/2010.00006) [astro-ph.GA]
- Poglitsch A, Waelkens C, Geis N, et al (2010) The Photodetector Array Camera and Spectrometer (PACS) on the Herschel Space Observatory. *Astronomy & Astrophysics* 518:L2. <https://doi.org/10.1051/0004-6361/201014535>, [arXiv:1005.1487](https://arxiv.org/abs/1005.1487) [astro-ph.IM]
- Preibisch T (2012) The reliability of age measurements for Young Stellar Objects from Hertzsprung-Russell or color-magnitude diagrams. *Research in Astronomy and Astrophysics* 12:1–25. <https://doi.org/10.1088/1674-4527/12/1/001>
- Price SD, Egan MP, Carey SJ, et al (2001) Midcourse Space Experiment Survey of the Galactic Plane. *Astronomical Journal* 121(5):2819–2842. <https://doi.org/10.1086/320404>
- Robitaille TP (2017) A modular set of synthetic spectral energy distributions for young stellar objects. *Astronomy & Astrophysics* 600:A11. <https://doi.org/10.1051/0004-6361/201425486>, [arXiv:1703.05765](https://arxiv.org/abs/1703.05765) [astro-ph.SR]
- Roy A, André P, Palmeirim P, et al (2014) Reconstructing the density and temperature structure of prestellar cores from Herschel data: A case study for B68 and

- L1689B. *Astronomy & Astrophysics* 562:A138. <https://doi.org/10.1051/0004-6361/201322236>, [arXiv:1311.5086](https://arxiv.org/abs/1311.5086) [astro-ph.GA]
- Sakai N, Honma M, Nakanishi H, et al (2012) Outer Rotation Curve of the Galaxy with VERA I: Trigonometric Parallax of IRAS 05168+3634. *Publ Astr Soc Japan* 64:108. <https://doi.org/10.1093/pasj/64.5.108>, [arXiv:1204.4782](https://arxiv.org/abs/1204.4782) [astro-ph.GA]
- Schlegel DJ, Finkbeiner DP, Davis M (1998) Maps of Dust Infrared Emission for Use in Estimation of Reddening and Cosmic Microwave Background Radiation Foregrounds. *Astrophysical Journal* 500(2):525–553. <https://doi.org/10.1086/305772>, [arXiv:astro-ph/9710327](https://arxiv.org/abs/astro-ph/9710327) [astro-ph]
- Siess L, Dufour E, Forestini M (2000) An internet server for pre-main sequence tracks of low- and intermediate-mass stars. *Astronomy & Astrophysics* 358:593–599. [astro-ph/0003477](https://arxiv.org/abs/astro-ph/0003477)
- Soderblom DR (2010) The Ages of Stars. *Ann Rev Astron Astrophys* 48:581–629. <https://doi.org/10.1146/annurev-astro-081309-130806>, [arXiv:1003.6074](https://arxiv.org/abs/1003.6074) [astro-ph.SR]
- Varricatt WP, Davis CJ, Ramsay S, et al (2010) A near-IR imaging survey of intermediate- and high-mass young stellar outflow candidates. *Mon Not R Astron Soc* 404(2):661–720. <https://doi.org/10.1111/j.1365-2966.2010.16356.x>, [arXiv:1001.2708](https://arxiv.org/abs/1001.2708) [astro-ph.SR]
- Wouterloot JGA, Brand J (1989) IRAS sources beyond the solar circle. I. CO observations. *Astronomy and Astrophysics Suppl Ser* 80:149–187
- Wright EL, Eisenhardt PRM, Mainzer AK, et al (2010) The Wide-field Infrared Survey Explorer (WISE): Mission Description and Initial On-orbit Performance. *Astronomical Journal* 140:1868–1881. <https://doi.org/10.1088/0004-6256/140/6/1868>, [arXiv:1008.0031](https://arxiv.org/abs/1008.0031) [astro-ph.IM]
- Wu YW, Reid MJ, Sakai N, et al (2019) Trigonometric Parallaxes of Star-forming Regions beyond the Tangent Point of the Sagittarius Spiral Arm. *Astrophysical Journal* 874(1):94. <https://doi.org/10.3847/1538-4357/ab001a>, [arXiv:1901.09313](https://arxiv.org/abs/1901.09313) [astro-ph.GA]
- Zhang Q, Hunter TR, Brand J, et al (2005) Search for CO Outflows toward a Sample of 69 High-Mass Protostellar Candidates. II. Outflow Properties. *Astrophysical Journal* 625(2):864–882. <https://doi.org/10.1086/429660>